ACCEPTED MANUSCRIPT

Published version available at: https://doi.org/10.1080/13647830.2021.1901996

Premixed flames in a narrow slot with a step-wise wall temperature: linear stability analysis and dynamics

Vadim N. Kurdyumov, Daniel Fernández-Galisteo and Carmen Jiménez

Department of Energy, CIEMAT, Avda. Complutense 40, 28040 Madrid, Spain

ARTICLE HISTORY
Compiled March 4, 2021

ABSTRACT
Premixed flames in a narrow slot with a prescribed wall temperature subject to a Poiseuille flow are investigated for various Lewis numbers within a constant density model and using irreversible Arrhenius kinetics. A global stability analysis of steady-state solutions is carried out together with time-dependent direct numerical simulations. The unsteady results are found in good agreement with the stability results. Additionally, it is demonstrated that for some values of the flow rate a multiplicity of time-periodic states can take place. The multiple time-periodic solutions arise from combinations of various unstable modes, symmetric and non-symmetric with respect to the channel midplane.

KEYWORDS
Premixed flame dynamics, Combustion instabilities, Non-symmetric flames, Micro-scale combustion, Heated channels

1. Introduction

The study of combustion processes in small-sized devices has recently received considerable attention. Details can be found in various reviews, see [1–6]. The practical relevance of this type of devices can be understood in at least two examples. The first example is a portable combustor for energy generation that could be used in remote conditions, far from standard energy sources, as an alternative to batteries. It is well known that the (chemical) energy capacity of any fuel is much higher than the capacity of conventional lithium batteries. And this is so even assuming a relatively low efficiency in the extraction of useful (electric) power in such devices.

Another type of small-sized device is a combustor suitable for burning low-energy-containing substances, super adiabatic combustors [7–9]. Direct combustion of such substances is hardly possible without additional heating. However, as shown in several studies, there is the possibility to organize heat fluxes in such a way that the temperature inside the device reaches a value notably higher than the corresponding adiabatic temperature of the mixture. This kind of devices include those used to produce hydrogen from hydrogen-containing fuels via reforming techniques [10, 11].

A common characteristic of the above devices is the narrowness of geometric dimensions, when combustion occurs in a narrow channel of width close to or slightly higher than the thermal flame thickness. This leads to a significant enhancement of

CONTACT V.N. Kurdyumov. Email: vadim.k@ciemat.es

@2020 This manuscript version is made available under the CC-BY-NC-ND 4.0 license: http://creativecommons.org/licenses/by-nc-nd/4.0/

@2020 This manuscript version is made available under the CC-BY-NC-ND 4.0 license: http://creativecom

heat exchange with the walls, the exterior of the device, or adjacent channels. A not very desirable consequence of large heat losses is the complication of conditions for stable operation of these systems. On the other hand, the narrowness of the channels is a necessary condition for maintaining super adiabatic temperatures in combustion zones.

The interest in these technologies has led to the emergence of interest in studying flames freely propagating in narrow channels. Generally speaking, the dynamics of flames in narrow channels turns out to be very diverse even under adiabatic conditions [12–15]. For example, the flame becomes asymmetric under certain conditions. Differential diffusion effects [12] or thermal expansion effects [15], can lead to the appearance of asymmetric flames differing significantly in characteristics from their symmetric counterparts. It must be pointed out that both the equations and the boundary conditions remain completely symmetric in these cases.

Another line of investigation focuses on premixed flames in narrow channels in the presence of an additional external flux of thermal energy, e.g. partially heated channels or channels with a prescribed wall temperature profile. This type of device has been the subject of many studies, numerical and analytical, as well as experimental, see [16–24], opening up wide opportunities for a detailed study of the chemical combustion reactions. An unexpectedly wide variety of different types of flame dynamics has been reported in this configuration.

It is important to remark a fundamental difference between the dynamics of freely propagating flames in channels [12–15] and that of flames in a channel with a prescribed temperature at the wall [16–24]. In the first case, the steady state solutions in the form of traveling waves are always invariant with respect to a shift along the direction of motion while in the second case this possibility is absent. An important distinctive feature is also the need to calculate the velocity of the combustion wave, that is, the eigenvalue of the problem, in the first case.

In the present work, the physical formulation of the problem is similar to that in [17], where a two-dimensional planar channel with a prescribed wall temperature was analyzed by means of direct numerical simulations within the constant density approximation and with the Lewis number equal to unity. Here, we extend that work to general three-dimensional simulations, including global stability analysis and the study of the influence of various parameters, such as the Lewis number and the temperature of the heated wall.

The article is arranged as follows. Sections 2 and 3 present the general formulation and the details of the linear global stability analysis. The numerical treatment is briefly described in Section 4. Numerical results are presented in Section 5, beginning with steady-state solutions. In order to comprehensively emphasize the impact of various parameters on the flame dynamics, the stability results and time-dependent dynamics are given and compared at the same time. This allows to validate the results using different approaches. Finally, a discussion on the results is presented in the last section

2. General formulation

Consider a combustible mixture at initial temperature T_0 flowing in a slot of height h between two parallel walls. A sketch of the geometry of the problem is given in Figure 1. We assume that the extent in the lateral direction is infinite, $-\infty < z' < \infty$. A step function for the wall temperature is used here in order to avoid introducing an additional length scale pertaining to the thickness of the ramping function. The

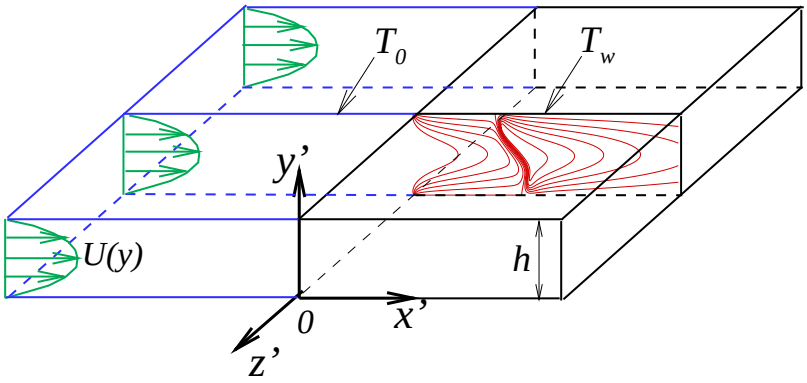

Figure 1. Sketch of the problem, coordinate system, velocity field and typical temperature contours.

wall temperature is fixed at T_0 for $x' < 0$ and at T_w for $x' > 0$, where $T_w > T_0$. Primes here and hereafter denote dimensional quantities if the same notation is used for dimensional and non-dimensional variables.

For the sake of simplicity, this work adopts a diffusive-thermal model, according to which the density of the mixture ρ, the heat capacity c_p, the thermal diffusivity $\mathcal{D}_T$, and the molecular diffusivity $\mathcal{D}$ are all assumed constant. Consequently, the flow field is not affected by combustion and the flow velocity is given by the Poiseuille flow, $u_x = 6U_0(1-y'/h)(y'/h)$, $u_y = u_z = 0$, where U_0 is the mean flow velocity. The effects of thermal expansion and variable transport properties will be reported elsewhere.

Despite the relevance of complex combustion chemistry, the chemical model of the present study is reduced to an irreversible single-step reaction of the form $\mathrm{F} + \mathrm{O} \rightarrow \mathrm{P} + Q$, where F denotes the fuel, considered to be the deficient reactant, O the oxidizer, P the products, and Q the heat released per unit mass of fuel. The combustion rate, Ω, is assumed to follow the Arrhenius law, $\Omega = \rho^2 \mathcal{B} Y \exp(-E/\mathcal{R}T)$, where ρ, $\mathcal{B}$, Y, E, $\mathcal{R}$ and T are the density, the pre-exponential factor, the fuel mass fraction, the activation energy, the universal gas constant and the temperature of the mixture, respectively. The mass fraction of the excess oxidizer is assumed to remain constant, and is therefore included in the value of pre-exponential factor $\mathcal{B}$.

The nondimensional temperature is defined as $\theta = (T - T_0)/(T_e - T_0)$, where $T_e = T_0 + QY_0/c_p$ is the adiabatic temperature of the corresponding planar flame based on the upstream fuel mass fraction Y_0. Similarly, $\theta_w = (T_w - T_0)/(T_e - T_0)$ is the non-dimensional temperature of the hot section of the wall. Choosing the channel height h as the reference length scale, $x = x'/h$, $y = y'/h$, $z = z'/h$, and using $h^2/\mathcal{D}_T$ and Y_0 to normalize the time and the mass fraction, respectively, the system is modeled as

$$\frac{\partial \theta}{\partial t} + 6m\sqrt{d}\, y(1-y)\frac{\partial \theta}{\partial x} = \Delta\theta + d \cdot \omega, \tag{1}$$

$$\frac{\partial Y}{\partial t} + 6m\sqrt{d}\, y(1-y)\frac{\partial Y}{\partial x} = \frac{1}{Le}\Delta Y - d \cdot \omega, \tag{2}$$

where $\Delta = \partial^2/\partial x^2 + \partial^2/\partial y^2 + \partial^2/\partial z^2$ is the Laplace operator and

$$\omega = \frac{\beta^2}{2Le\, u_p^2} Y \exp\left\{\frac{\beta(\theta-1)}{1+\gamma(\theta-1)}\right\} \tag{3}$$

is the non-dimensional reaction rate.

The planar burning velocity, S_L, and the thermal flame thickness, defined as $\delta_T = \mathcal{D}_T/S_L$, are used in order to specify the non-dimensional parameters appearing in the formulation: the reduced Damköhler number, $d = h^2/\delta_T^2 = h^2 S_L^2/\mathcal{D}_T^2$, and the non-dimensional flow velocity, $m = U_0/S_L$. The remaining dimensionless parameters are the Zel'dovich number, $\beta = E(T_e - T_0)/\mathcal{R}T_e^2$, the Lewis number, $Le = \mathcal{D}_T/\mathcal{D}$, and the heat release parameter, $\gamma = (T_e - T_0)/T_e$.

The factor $u_p = S_L/U_L$ appearing in Eq. (3) has been introduced to account for the difference between the asymptotic value of the laminar flame speed,

$$U_L = \sqrt{2\rho\mathcal{B}\mathcal{D}_T Le\beta^{-2}}\exp\left(-E/2\mathcal{R}T_e\right),$$

obtained for large activation energy ($\beta \gg 1$) and the numerical value S_L calculated for a finite β. The factor u_p ensures that for a given β the non-dimensional speed of a planar adiabatic flame equals one. Clearly, the factor u_p tends to one when $\beta \to \infty$. The numerical values of u_p were reported in [12] as a function of the Lewis number for $\beta = 10$ and $\gamma = 0.7$. These values are kept as representative values in the present study.

The boundary conditions for the temperature and mass fraction are imposed as follows:

$$y = 0 \text{ and } y = 1: \quad \partial Y/\partial y = 0, \quad \theta = \begin{cases} \theta_w, & x > 0, \\ 0, & x < 0; \end{cases} \tag{4}$$

$$x \to -\infty: \quad \theta \to 0, \quad Y \to 1; \quad x \to \infty: \quad \partial^2 Y/\partial x^2 = \partial^2\theta/\partial x^2 = 0. \tag{5}$$

It is assumed that the slot is infinite in the z-direction and standard periodic conditions are applied at the lateral boundaries when it is required.

Weak boundary conditions for the temperature and mass fraction including zero values of the second derivatives were used downstream. This allowed for a shorter computational domain. Nevertheless, the numerical simulations reported below showed that the influence of the downstream boundary conditions becomes negligible if the size of the computational domain is sufficiently large. The same boundary conditions were applied in [13, 25].

It is important to note that Eqs. (1)-(2) together with Eqs. (4)-(5) are symmetric with respect to the channel midplane $y = 1/2$, say, to the transformation $y \to 1 - y$. Consequently, calculations of symmetric solutions can always be forced by reducing the domain to half of its height, $0 \le y \le 1/2$, and imposing symmetric boundary conditions in the form

$$y = 1/2: \quad \partial\theta/\partial y = \partial Y/\partial y = 0. \tag{6}$$

In order to identify the symmetry of solutions computed in the entire domain,

$0 \leq y \leq 1$, the symmetry indicator

$$S(z,t) = \int_{-\infty}^{\infty} dx \int_{0}^{1/2} [\theta(x,y,z,t) - \theta(x,1-y,z,t)]dy \tag{7}$$

is used. Clearly, $S \equiv 0$ (within numerical accuracy) for a symmetric solution and $S \neq 0$ when it is non-symmetric. Evidently, for every non-symmetric solution there is a mirror one obtained by a $y \to 1-y$ transformation for which the symmetry indicator S changes only its sign.

The flame position, $x_w(z,t)$, is defined as the point along the line $y = 1/2$ and $z = const$ where the reaction rate reaches its maximum value, $\omega|_{x=x_w} = \omega_{max}$. Even though this characteristic does not fully reflect the position of the flame, because the flame may have perceptible curvature, x_w will be used below to characterize the flame. Determining the flame position in this way makes sense in not very wide channels. The quantities S and x_w become independent of z in the case of planar solutions (i.e. when all distributions are independent on z).

3. Mathematical background of stability analysis

Steady as well as time-dependent computations were carried out in the present study. For the two-dimensional (independent of z) steady-state solutions, a numerical global stability analysis was carried out. Knowing the stability properties of steady-state solutions, even in cases where they are unstable and cannot be implemented in practice, allows a better understanding of the unsteady flame dynamics. The corresponding procedure is quite standard and is given below for the sake of completeness. The numerical method for the stability analysis used here follows that proposed in [12]. This method allows to calculate the eigenvalue with the largest real part.

Two-dimensional steady-state distributions of the temperature and mass fraction, all now denoted by the subindex 0, are perturbed as usual with small perturbations

$$\begin{array}{l} \theta = \theta_0(x,y) + \epsilon\Phi(x,y)\exp(\lambda t + ikz) \\ Y = Y_0(x,y) + \epsilon\Psi(x,y)\exp(\lambda t + ikz) \end{array} \tag{8}$$

where λ is a complex number, the real part of which, λ_R, represents the growth rate, k is the wavenumber in the transversal direction z, and ϵ is a small amplitude. The linearized eigenvalue problem obtained when substituting Eq. (8) into Eqs. (1)-(2) reduces to finding non-trivial solutions of the two-dimensional system

$$\lambda\Phi + 6m\sqrt{d}y(1-y)\frac{\partial\Phi}{\partial x} = \frac{\partial^2\Phi}{\partial x^2} + \frac{\partial^2\Phi}{\partial y^2} - k^2\Phi + d(A\Phi + B\Psi)\,, \tag{9}$$

$$\lambda\Psi + 6m\sqrt{d}y(1-y)\frac{\partial\Psi}{\partial x} = \frac{1}{Le}\left(\frac{\partial^2\Psi}{\partial x^2} + \frac{\partial^2\Psi}{\partial y^2} - k^2\Psi\right) - d(A\Phi + B\Psi)\,, \tag{10}$$

where

$$A = \frac{\beta^3 Y_0}{2Le\, u_p^2[1+\gamma(\theta_0-1)]^2} \exp\left\{\frac{\beta(\theta_0-1)}{1+\gamma(\theta_0-1)}\right\}, \quad B = \frac{\beta^2}{2Le\, u_p^2} \exp\left\{\frac{\beta(\theta_0-1)}{1+\gamma(\theta_0-1)}\right\} \tag{11}$$

are both functions of x and y.

The corresponding boundary conditions for the perturbations at the wall are

$$y = 0 \text{ and } y = 1: \quad \Phi = \partial\Psi/\partial y = 0. \tag{12}$$

In order to study the stability of the symmetric steady states, Eqs. (9)-(10) should be considered in the half-height domain, $0 \le y \le 1/2$, along with two kinds of boundary conditions at the channel midplane selecting either symmetric or non-symmetric modes

$$\text{symmetric mode:} \quad \partial\Phi/\partial y = \partial\Psi/\partial y = 0 \quad \text{at} \quad y = 1/2; \tag{13}$$

$$\text{non-symmetric mode:} \quad \Phi = \Psi = 0 \quad \text{at} \quad y = 1/2. \tag{14}$$

4. Numerical treatment

Steady as well as time-dependent computations were carried out in a finite domain, $x_{min} < x < x_{max}$. The size of the domain was significantly varied in order to verify the independence of the results. In the case of three-dimensional computations, the domain size was also finite in the z-direction, $0 < z < z_{max}$, with periodic boundary conditions. The spatial derivatives were discretized on a uniform grid using second order, three-point central differences. The typical number of grid points was 1001×101 in the (x, y) directions for two dimensional calculations and $801 \times 81 \times 401$ along the (x, y, z) axes for three dimensional ones. The number of grid points was doubled in some cases without significant differences in the results.

For unsteady calculations an explicit marching procedure was used with first order discretization in time. The typical time step was $\tau = O(10^{-5})$. No significant differences were found in the results when τ was halved. In order to determine steady (but not necessary stable) solutions, the steady counterpart ($\partial/\partial t = 0$) of Eqs. (1) and (2) was solved using a Gauss-Seidel method with over-relaxation.

It should be noted that in calculating steady-state solutions ($\partial/\partial t = 0$ imposed), the grid size affected the solutions only moderately, after a certain minimum grid size was chosen. However, when calculating time-dependent solutions, the influence of spatial resolution turned out to be very significant on the flame dynamics. In some cases, the flame dynamics obtained on coarse grids turned out to be completely different from the real dynamics (obtained on a finer grid), while the corresponding steady-state distributions calculated on fine and coarse grids turned out to be very close to each other. This remark relates mainly to the calculation of three-dimensional cases. The fact is that in three-dimensional calculations, an increase in spatial resolution (a finer grid step) is accompanied by a significant increase in computational costs. The effect of grid coarseness was also detected in the results of linear stability analysis, which were obtained using a quasi time-dependent method [12]. However, in this case this was not so critical, since an increase in accuracy was achieved with little increase in computational cost.

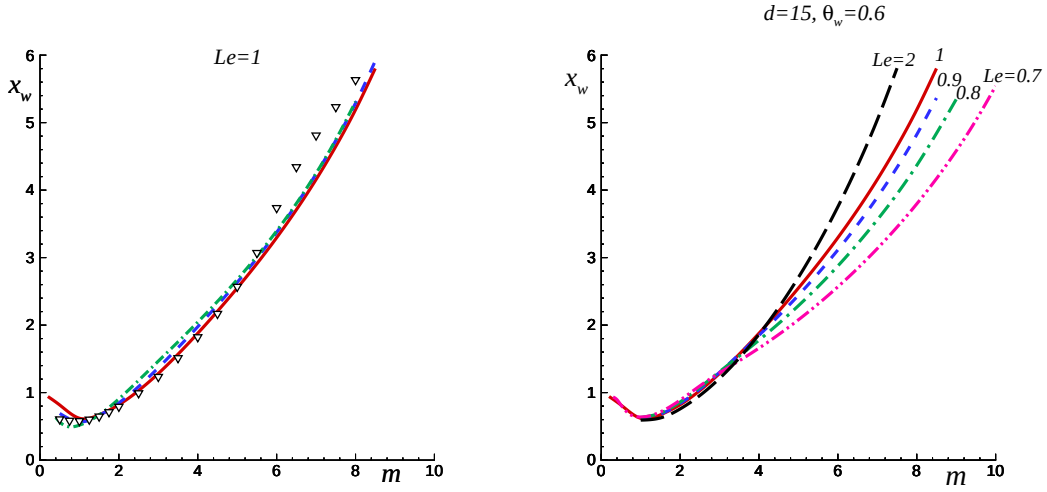

Figure 2. Left plot: the steady-state flame position x_w versus the non-dimensional flow rate m: solid, dashed and dash-dot lines are $d = 15$, 20 and 30, respectively, all for $\theta_w = 0.6$; triangles - $d = 15$ and $\theta_w = 0.7$. Right plot: the steady-state flame position as a function of the flow rate for various Le; calculated for $d = 15$ and $\theta_w = 0.6$.

5. Numerical results

The flame behavior in channels depends primarily on the channel width and the temperature conditions on the wall. In adiabatic channels (no heat-losses), the flame propagation is possible at any channel width both upstream (flame flashback) and downstream (flame blow off), depending on the mixture flow rate. In the presence of heat losses, there is a critical value of the channel width below which the flame is extinguished.

This study examines the flame behavior in channels with a fixed temperature distribution on the wall, given by a step function. The upstream wall temperature is kept cold so that upstream flame propagation is only possible in a sufficiently wide channel. On the other hand, the downstream wall temperature is chosen high enough and the downstream flame motion (blowing the flame off) becomes just as difficult. These two conditions result in the flame being situated/located in the zone near the temperature jump.

5.1. Symmetric two-dimensional steady-state solutions

It should be noted that a steady-state, two-dimensional (independent of z) and symmetric with respect to the $y = 1/2$ midplane solution of Eqs. (1)-(5) always exists, at least as a mathematical object. Despite the fact that these solutions are often unstable, information about them and their structure is always useful to understand, for example, the dynamics of unsteady solutions, which oscillate around these solutions. This facilitates the interpretation of the results of time dependent simulations in a parametric space.

The dependence of x_w on m calculated for $Le = 1$ in a two-dimensional domain is shown in Fig. 2 (left plot). The cases with $d = 15$, 20 and 30 calculated for $\theta_w = 0.6$ are shown with solid, dashed and dash-dot lines, respectively, and triangles correspond to the case with $d = 15$ and $\theta_w = 0.7$. It can be seen that with variations of d, the flame position x_w varies only slightly if m is fixed. Perhaps the difference will be more

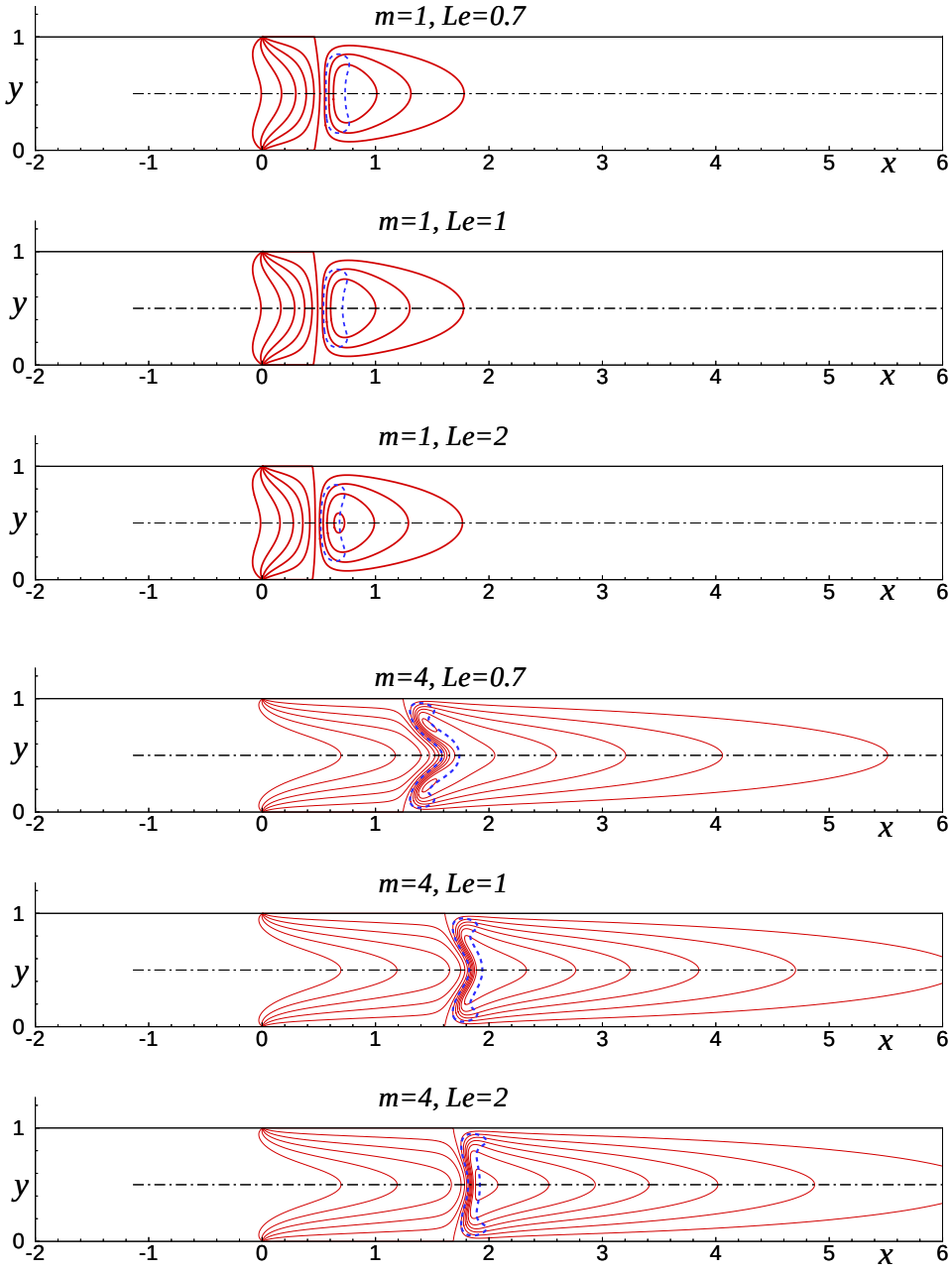

Figure 3. Flame structures for symmetric planar flames for various Le and various m; all cases were calculated with $d = 15$ and $\theta_w = 0.6$; solid lines show isotherms plotted at interval 0.1; a dashed line shows an isoline of the reaction rate with $\omega = 10$.

noticeable for larger d.

The dependence of x_w on m for various values of Le calculated for $d = 15$ and $\theta_w = 0.6$ is shown in Fig. 2 (right plot). A moderate effect of the Lewis number is detected for large values of m, while for m near unity the curves coincide noticeably. This can be clarified by considering flame structures at different Lewis numbers and mixture flow rates.

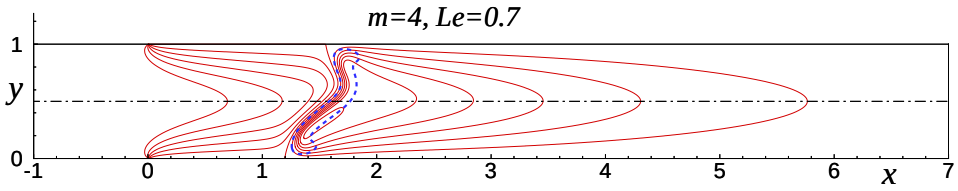

Figure 4. An example of a planar steady-state nonsymmetric solution calculated for $m = 4$ and $Le = 0.7$ corresponding to the open circle in Fig. 5; isotherms plotted with solid lines at interval 0.1; a dashed line in all plots shows an isoline of the reaction rate with $\omega = 10$.

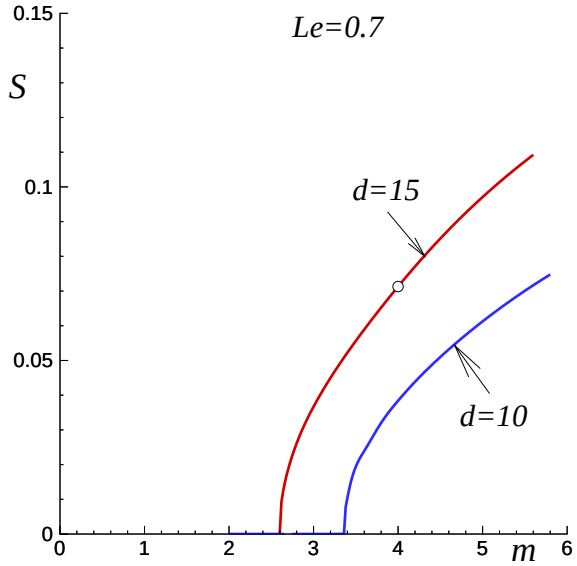

Figure 5. Examples of supercritical bifurcations of planar solutions illustrated by the symmetry indicator, S, versus the flow rate, m, calculated for $Le = 0.7$ and $\theta_w = 0.6$.

Examples of the flame structure for two values of m and several values of Le are illustrated in Fig. 3 where the temperature distributions were calculated for $d = 15$, $\theta_w = 0.6$. One can see that when the flow rate of the mixture is not large (e. g. $m = 1$), the temperature distributions are very similar for all Lewis numbers. The temperature reaches its maximum value in the midplane of the channel. However, at relatively high flow velocities (e. g. $m = 4$) a qualitative change in the flame structure occurs. The temperature maximum shifts toward the channel wall for $Le = 0.7$, while for $Le \geqslant 1$ the temperature maximum continues to be in the midplane of the channel. These features of the flame structure affect the stability properties.

5.2. Nonsymmetric two-dimensional steady-state solutions

All cases of steady-state solutions presented so far have been obtained by calculations in a half-domain, $0 < y < 1/2$, with symmetry conditions at the midplane using the Gauss-Seidel method ($\partial/\partial t = 0$ imposed). It was verified that for $Le \geqslant 1$ the steady-state calculations in the entire domain gave exactly the same solutions. No non-symmetric steady-state solutions were found for $Le \geqslant 1$. Interestingly, if these calculations are performed for $Le < 1$ in the entire domain, $0 < y < 1$, steady-state nonsymmetric solutions appear at sufficiently high flow rates. An example of this type of solution is shown in Fig. 4 for $m = 4$, $d = 15$ calculated for $Le = 0.7$.

These steady-state nonsymmetric solutions emerge as a result of the supercritical bifurcation of a symmetric solution (at least in the considered range of parameters) when the flow intensity exceeds a critical value. Obviously, for each nonsymmetric solution there exists a mirror-symmetric counterpart by means of the $y \to 1 - y$ transformation. The bifurcation point depends on the channel width. Figure 5 shows the symmetry index S as a function of the flow rate for two channel widths. As expected, in narrower channels the nonsymmetric solutions appear at higher flow rates. Anticipating the results of global stability analysis, it must be mentioned that these solutions are also unstable with respect to disturbances in the z-direction, forming a cellular structure in this direction.

5.3. Stability and dynamics of flames with $Le = 1$

It should be noted that the appearance of cellular or oscillatory instabilities for planar and freely propagating flames occurs when the Lewis number is below or above a threshold value which depends on β and γ. For the values $\beta = 10$ and $\gamma = 0.7$ used in the present study the instabilities of freely propagating planar flames occur if $Le \lesssim 0.84$ (cellular) and $Le \gtrsim 3.59$ (oscillatory), see [25].

Consider now the flames with $Le = 1$. The above steady-state symmetric solutions were investigated for stability. The growth rate, λ_R, and the corresponding frequency, λ_I, were calculated separately for symmetric and non-symmetric perturbations controlled by the boundary conditions at the midplane given by Eq. (13)-(14).

Figure 6 shows λ_R as a function of the transverse wave number k for $d = 15$, $\theta_w = 0.6$ and several m. The growth rates of symmetric and nonsymmetric modes are plotted with solid and dashed lines, respectively. One can see that for all cases the maximum value of λ_R is achieved at $k = 0$. This means that the most unstable mode corresponds to planar perturbations (independent of z).

The growth rate λ_R calculated for $k = 0$ is given in Fig. 7 as a function of m for $d = 15$ and two values of the wall temperature. The solid lines correspond to the symmetric mode and the dashed lines to the nonsymmetric mode.

Consider first the case with $\theta_w = 0.6$. Figure 7 shows that the symmetric mode, being stable at low m, becomes unstable within the interval $0.367 \lesssim m \lesssim 1.89$. However, with increasing m, re-stabilization occurs. With a further increase in the flow rate both the symmetric and nonsymmetric modes lose stability when m exceeds the critical (different) values of $m_c \approx 3.17$ and $m_c \approx 3.06$, respectively.

The growth rates reach their maximum values for some m, after which their magnitudes decrease. The flame stabilizes when the flow intensity exceeds $m_c \approx 8.02$. It should be noted that the values of λ_R calculated for the symmetric and nonsymmetric modes become close to each other for large m. The critical values of m above which the flame becomes stable are also very close for symmetric and nonsymmetric

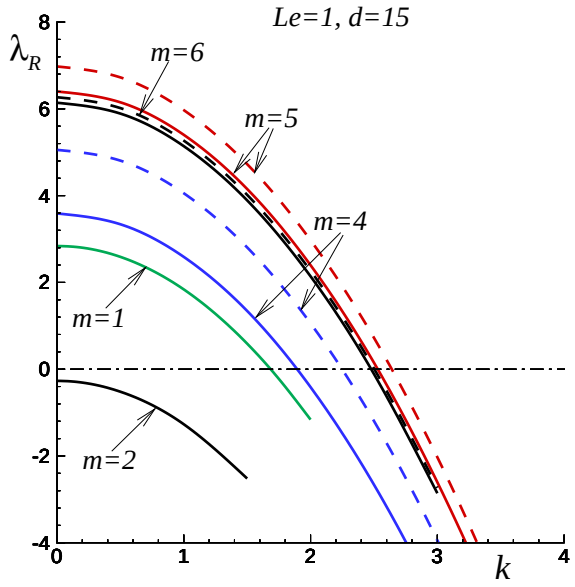

Figure 6. The dependence of λ_R on the wave number k; the solid curves calculated for the symmetric perturbations and the dashed curves for the non-symmetric perturbations; all curves for $Le = 1$, $d = 15$ and $\theta_w = 0.6$.

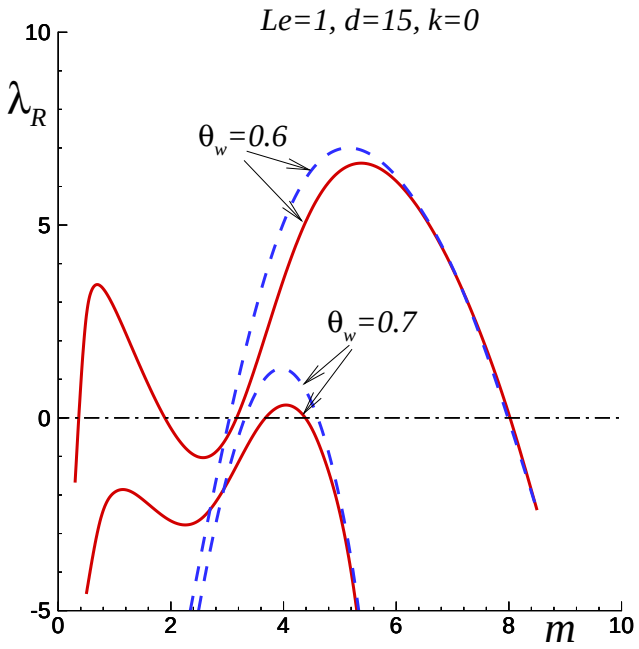

Figure 7. The dependence of λ_R on the flow rate m calculated for planar perturbations, $k = 0$; the solid curves calculated for the symmetric perturbations and the dashed curves for the non-symmetric perturbations.

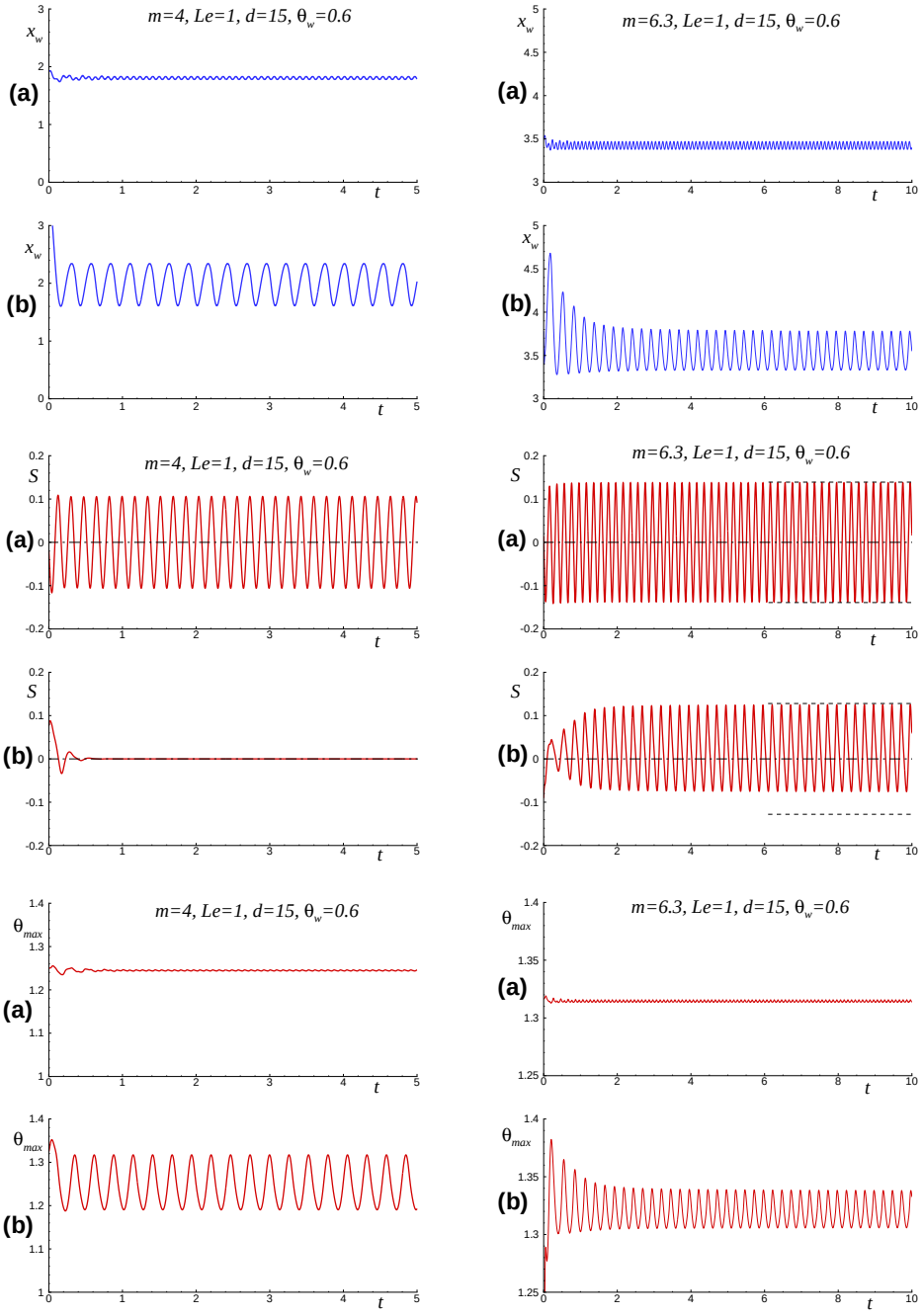

Figure 8. Time history of the flame position x_w, the symmetry indicator S and the maximum temperature calculated over the entire channel, θ_{max}, computed for planar solutions for $m = 4$ (left column of plots) and $m = 6.3$ (right column of plots); all cases for $d = 15$ and $\theta_w = 0.6$.

perturbations.

It was this flame behavior that was reported in [17], where the unsteady flame dynamics was explored using two-dimensional direct time-dependent simulations. Evidently, the exact determination of the critical values at which the flame dynamics changes by means of time-dependent simulations can face difficulties, while a reason-

able accuracy is achieved here by the stability analysis.

Time-dependent calculations were performed to validate the results of the stability analysis. It is remarkable that when the symmetric and nonsymmetric modes are both unstable, two different types of oscillatory dynamics are observed for the same set of parameters. Figure 8 shows the values of the flame position, x_w, the symmetry indicator, S, and the maximum temperature calculated over the entire channel, θ_{max}, as functions of time for $m = 4$ (left column of plots) and $m = 6.3$ (right column of plots).

Consider the case with $m = 4$ shown in the left column of plots of Fig. 8. Two different oscillatory states are sustained in time. The first state, marked with (a), is characterized by a small amplitude of oscillations of the flame position x_w and a significant amplitude of the symmetry index S. Fluctuations in the maximum temperature are also small after a certain transition time during which the periodic dynamics is establishing. This state is clearly linked to the unstable nonsymmetric mode.

The second state found for $m = 4$, marked with (b) in Fig. 8 (left column), is characterized by significant oscillatng amplitudes of both the flame position and the maximum temperature, while the symmetry index is maintained equal to zero (after a transitional time). Obviously, this oscillatory state occurs upon excitation of the unstable symmetric mode. It is a surprising fact that these two unstable modes do not seem to interact with each other, at least for the present values of the parameters ($m = 4$). It must be emphasized that the calculations were carried out for a time significantly longer than that shown in Fig. 8. This gives confidence to conclude that these oscillatory states are sustained over time.

With increasing m, see the right column of plots in Fig. 8 where the case $m = 6.3$ is shown, the flame dynamics becomes even more interesting. It can be seen that one of the oscillating states (marked with (a)) corresponds to the pure nonsymmetric perturbation mode: significant fluctuations in the symmetry index and small fluctuations in the flame position confirm this. The oscillations of the symmetry index S occur in a symmetrical manner: the absolute maximum and minimum values of the symmetry indicator achieved during the oscillation period are equal, $|S_{max}| \approx |S_{min}|$, within numerical accuracy.

The other oscillatory state (indicated with (b)) is markedly different. Indeed, it can be seen that the oscillations of the symmetry index occur asymmetrically: the absolute maximum value differs from the absolute minimum value, $|S_{max}| \neq |S_{min}|$. The thin horizontal lines in the figure mark the quantities S_{max} and $-S_{max}$. One can assume that in this case two unstable modes interact with each other. This leads to the flame oscillations occurring asymmetrically relative to the channel midplane. An example of such oscillations is also included in the supplementary material. Numerical calculations showed that this mode disappears for large values of m and only the mode with purely symmetric oscillations ($|S_{max}| = |S_{min}|$) survives.

Figure 9 shows the magnitude of the frequency of oscillations, λ_I, calculated for $d = 15$ and $\theta_w = 0.6$. The solid and dashed lines correspond to the symmetric and nonsymmetric mode, respectively, obtained from the stability analysis. The circles show the frequencies evaluated from the unsteady calculations. Vertical lines indicate the boundaries of the stable/unstable intervals.

It can be seen that the frequencies obtained from time-dependent calculations coincide with great accuracy with λ_I obtained from the stability analysis when m is lying in the stable regions. In this case, the frequency is extracted from the oscillatory attenuation of the initial perturbations, see [26]. In unstable regions the real frequencies of oscillations differ from those of the stability analysis due to effects of nonlinearity. At

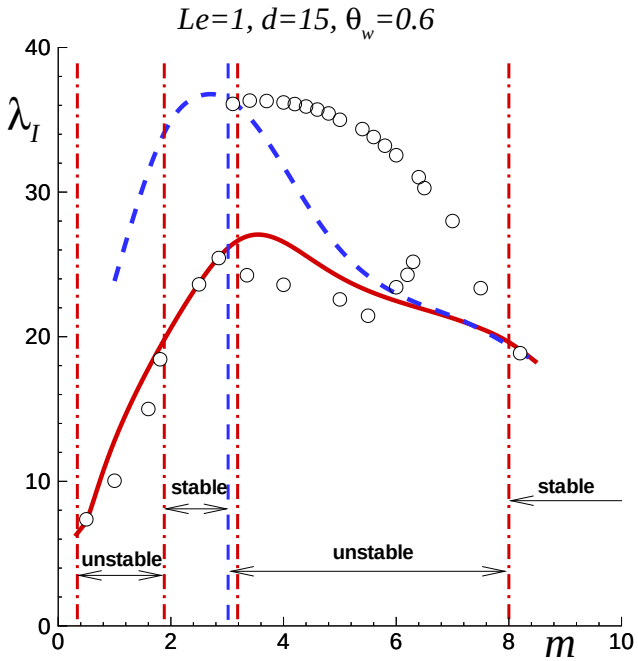

Figure 9. The frequency of oscillations λ_I calculated for $d = 15$ and $\theta_w = 0.6$; solid line - symmetric mode, dashed line - nonsymmetric mode; circles - unsteady simulations.

the same time, it can be seen that when two types of oscillations exist simultaneously, their respective frequencies differ noticeably from each other.

The appearance of oscillatory solutions substantially depends on the intensity of wall heating. The stability results shown in Fig. 7 indicate that with an increase in the wall temperature the steady-state solution is stabilized. The instability interval is greatly reduced at $\theta_w = 0.7$ and completely disappears at slightly larger values of the wall temperature. Here it must be remembered that the dimensionless temperature was introduced on the basis of the adiabatic temperature of a planar freely propagating flame.

Fig. 10

In Fig. 10, the values of λ_R computed for $d = 30$, $k = 0$ and two values of θ_w are plotted for the symmetric (solid line) and nonsymmetric (dashed line) modes. With increasing channel width, or, equivalently, for larger values of $d = h^2/\delta_T^2$, the degree of instability increases, as the case with $\theta_w = 0.6$ shows. The growth rate for symmetric and nonsymmetric modes becomes almost the same for large m. This figure also illustrates once again the influence of the wall temperature on flame oscillations: the region of instability practically disappears for $\theta_w = 0.7$. Although the study of the influence of θ_w has not been carried out in an exhaustive way, it can be concluded that an increase in θ_w leads to the stabilization of the flame.

Up to this point, all time-dependent calculations were carried out in the two-dimensional framework, namely by imposing $\partial/\partial z = 0$ in Eqs. (1)-(2). Three-dimensional time-dependent numerical calculations were performed in a finite domain, $0 < z < z_{max}$, with $z_{max} = 5 \div 10$. Standard periodic boundary conditions were used

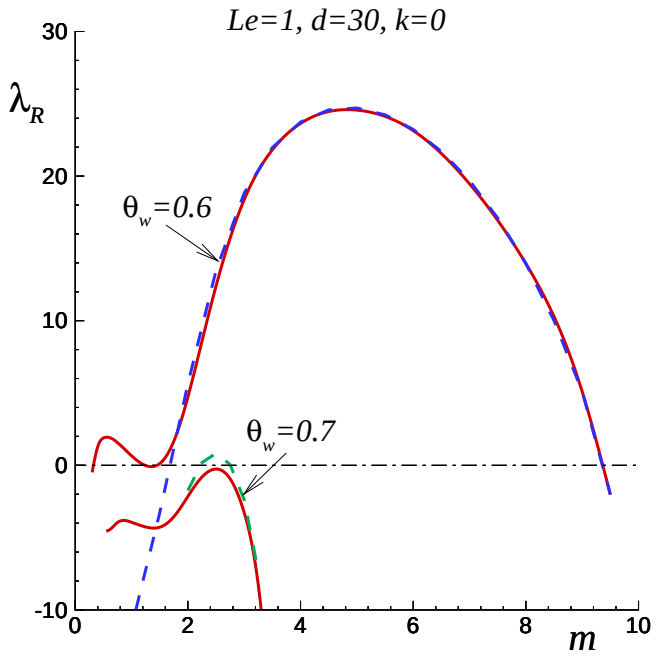

Figure 10. The growth rate λ_R for planar perturbations ($k = 0$): solid lines - symmetric modes, dashed lines - nonsymmetric modes; all curves for $Le = 1$, $d = 30$.

in the z-direction. The initial temperature distribution was chosen as follows

$$t = 0: \quad \theta(x, y, z) = \theta_{2D}(x, y)[1 + a\cos(2\pi n z/z_{max})\exp(-|x - x_*| - |y - y_*|)],$$

where $\theta_{2D}(x, y)$ is the temperature distribution (steady-state or instantaneous) obtained from two-dimensional calculations, with typical values $a = 0.3$ and $n = 1$ or 2. The value of $2\pi n/z_{max}$ corresponds to the transverse wave number k. The location for disturbances was chosen near the flame front, $x_* \approx x_w$, and $y_* \neq 1/2$ were used to get nonsymmetric initial conditions. The initial mass fraction distributions were taken directly from 2D calculations without perturbations.

Fig. 11

In order to analyze the flame dynamics in the three-dimensional case, we will use the flame position and the symmetry indicator in a plane $z = z_1$, together with the difference of these values in two planes z_1 and z_2: $\delta x_w = x_w(z_1, t) - x_w(z_2, t)$ and $\delta S = S(z_1, t) - S(z_2, t)$. Here z_1 and z_2 are some values from the interval $0 < z < z_{max}$. It is obvious that if δx_w and δS both tend to zero for any z_1 and z_2, the flame profile becomes independent of z. If, at the same time, S shows periodic oscillations, then the flame dynamics corresponds to a nonsymmetric unstable mode.

The results of 3D calculations showed that when the initial conditions depend on z, the flame dynamics for $Le = 1$ becomes independent of z after a transition time interval. Figure 11 shows the transition dynamics for the flame position and the symmetry indicator. The left and right columns correspond to cases of symmetric and non-symmetric oscillations, respectively. All curves were calculated for $m = 4$, $d = 15$

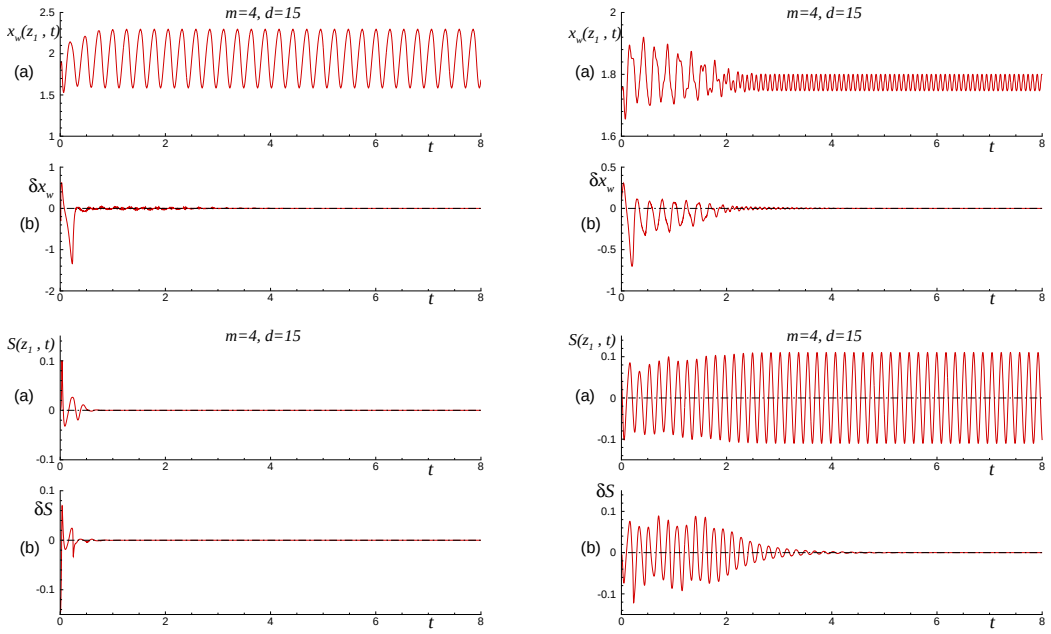

Figure 11. Transient 3D flame dynamics for symmetric (left plots) and non-symmetric (right plots) flame oscillations. Plots (a): time histories of the flame position, x_w, and the symmetry indicator, S, in a plane $z = z_1$; plots (b): time history of the differences $\delta x_w = x_w(z_1, t) - x_w(z_2, t)$ and $\delta S = S(z_1, t) - S(z_2, t)$ evaluated in two planes; all curves computed for $m = 4$, $d = 15$ and $\theta_w = 0.6$.

and $\theta_w = 0.6$, the same parameters used in Fig. 8 (left). It can be seen that while x_w and S are approaching their final periodic states, the differences between these values evaluated in two different planes, δx_w and δS, tend to zero. This means that the entire distributions become independent of z, that is, the flame becomes two-dimensional. This result confirms the conclusion that was drawn from the linear global stability analysis, namely, that the most unstable perturbation mode is the planar mode, $k = 0$.

5.4. Stability and dynamics of flames with $Le > 1$

Numerical calculations of the stability curves for flames with $Le > 1$ showed that the dependence on the wave number k is similar to that shown in Fig. 6 for $Le = 1$. The maximum value of the growth rate, λ_R, is achieved at $k = 0$, which corresponds to planar (independent of z) perturbations. This was observed for both symmetric and non-symmetric modes.

Figure 12 shows the growth rate λ_R (left plot) and the frequency of oscillations λ_I (right plot, only for $Le = 1.2$) as functions of the flow rate m calculated for $k = 0$, $d = 15$, $\theta_w = 0.6$ and various $Le > 1$. For comparison, the curves for $Le = 1$ are also shown. For all the cases given in the figure, the eigenvalue has a nonzero imaginary part λ_I.

One can see in the left plot of Fig. 12 the great sensitivity of the stability properties to variations of the Lewis number. For the symmetric mode (solid curves), the positive value of the second maximum of λ_R reached at $m \approx 5.3$ for $Le = 1$ becomes negative already for $Le = 1.2$. For non-symmetric perturbations (dashed curves), the maximum value of λ_R also decreases rapidly and also becomes negative with increasing values

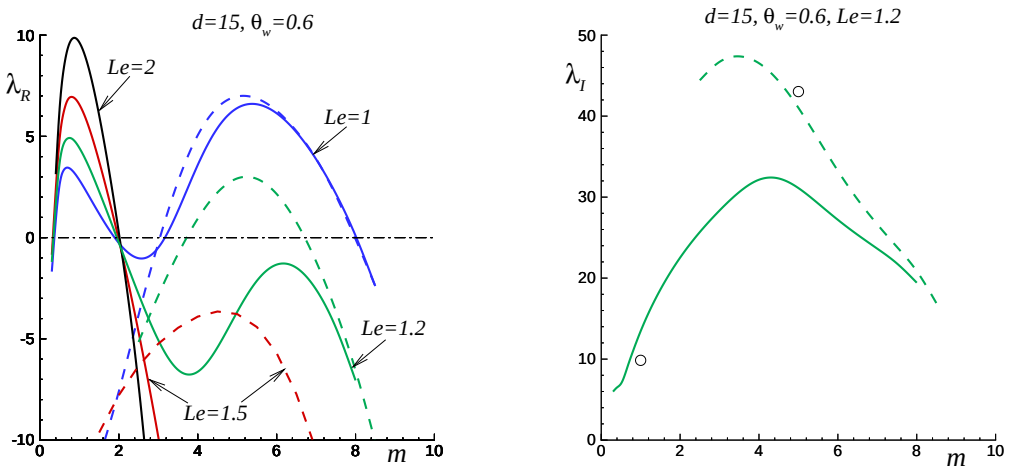

Figure 12. The growth rate of perturbations λ_R (left plot) and the frequency λ_I (right plot, only for $Le = 1.2$) for $d = 15$, $\theta_w = 0.6$ and various $Le \geq 1$; open circles in the right plot - the oscillation frequencies evaluated from time-dependent simulations shown in Fig. 13.

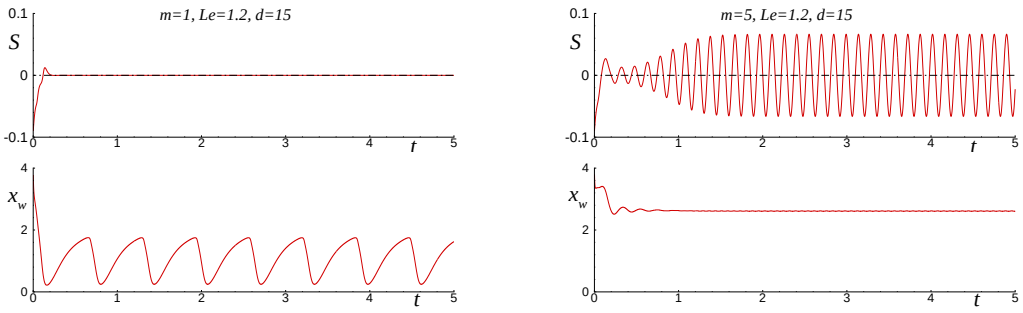

Figure 13. Time history of the symmetry indicator and the flame position for $Le = 1.2$, $d = 15$ and two values of m corresponding to circles in Fig. 12: the left plot - symmetric oscillations, the right plot - nonsymmetric oscillations.

of the Lewis number. On the other hand, the magnitude of the first maximum of λ_R occurring at low m increases with increasing Le. From these stability curves, it can be concluded that flame stabilization occurs at high flow rates m if the Lewis number even slightly exceeds unity. At the same time, one can observe an increase in the degree of instability at moderate flow rates, $m \sim 1$, when the Lewis number increases.

Figure 13 shows time histories of the symmetry index and flame position for $Le = 1.2$ and two values of m. A symmetric oscillatory behavior develops for $m = 1$ and non-symmetric oscillations occur for $m = 5$, in accordance with the stability curves. The frequencies of oscillations evaluated from these simulations are marked with circles in Fig. 12 (right). One can see that unsteady results are in good agreement with those of stability analysis.

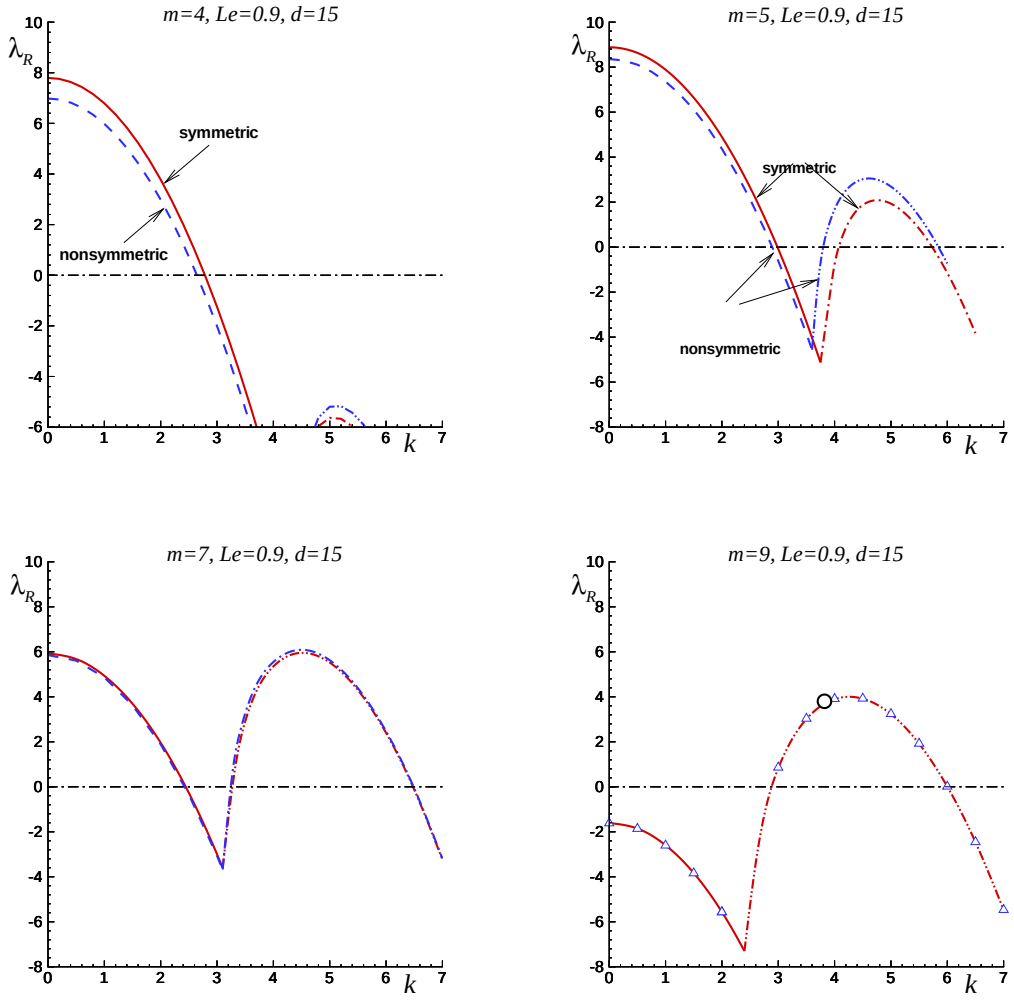

Figure 14. The growth rate λ_R as a function of the wave number k for several values of m and $Le = 0.9$, $d = 15$ and $\theta_w = 0.6$; solid and dashed lines - symmetric and nonsymmetric perturbations with $\lambda_I \neq 0$ (oscillatory modes); dash-dot and dash-dot-dot lines - symmetric and nonsymmetric perturbations with $\lambda_I = 0$ (cellular modes). For $m = 9$ the nonsymmetric mode is show with open triangles; an open circle in the plot for $m = 9$ shows the perturbation mode found in the three-dimensional calculations illustrated in Fig. 16.

5.5. Stability and dynamics of flames with Le < 1

It is well known that cellular thermodiffusion-induced instabilities can occur for freely propagating flames with Lewis numbers less than one. The eigenvalue of perturbations, λ, becomes purely real for $Le < 1$, reaching its maximum value, $\lambda = \lambda_{max}$, at a certain nonzero value of the wave number, $k = k_c$. If $\lambda_{max} > 0$ the magnitude of $\ell = 2\pi/k_c$ determines the characteristic size of disturbance cells. Given that $\lambda_I = 0$, there are no oscillations at the same time.

In the case of a narrow slot with heated walls, thermodiffusion-induced oscillatory instabilities occur even for $Le = 1$. One can expect that when the Lewis number decreases below unity, the cellular instability will also be present. The stability analysis of steady-state solutions showed their extreme sensitivity to the Lewis number in the

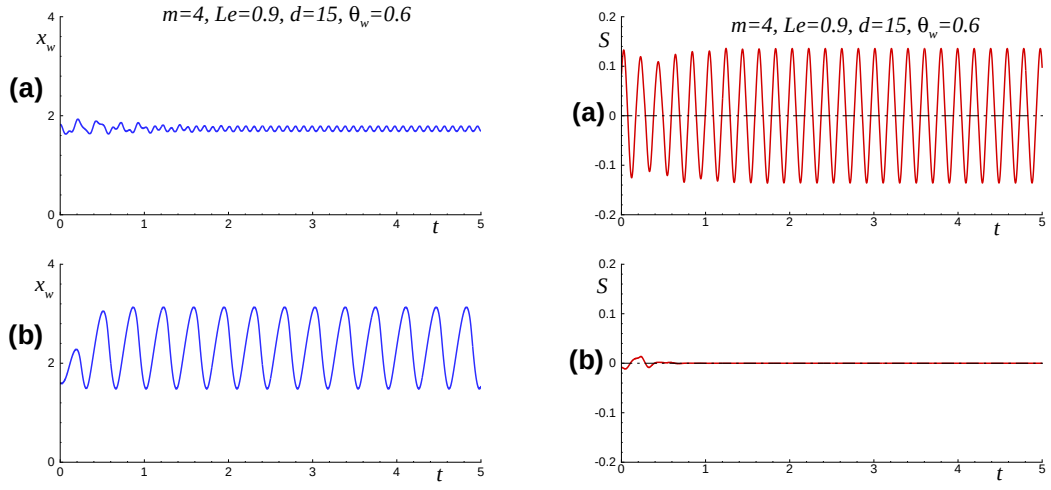

Figure 15. Time history of the flame position x_w (left plots) and the symmetry indicator S (right plots) computed for $m = 4$ and $Le = 0.9$ illustrating nonsymmetric (a) and symmetric (b) oscillations; all cases for $d = 15$ and $\theta_w = 0.6$.

present configuration when Le decreases below unity.

Figure 14 shows λ_R as a function of the wave number k for a case when the Lewis number is only slightly less than unity, for $Le = 0.9$, and several values of m. All calculations were carried out for $d = 15$ and $\theta_w = 0.6$. The solid and dashed lines correspond to symmetric and nonsymmetric perturbations, respectively, when the imaginary part of the eigenvalue, λ_I, is not zero (oscillatory instability). The dash-dot and dash-dot-dot lines correspond to symmetric and non-symmetric perturbations when $\lambda_I = 0$ (cellular instability).

Figure 14 shows that at moderate values of the flow rate (the case $m = 4$), the stability properties resemble those of the case $Le = 1$: the most unstable mode is the planar one corresponding to $k = 0$. The modes of cellular instability appearing at large k remain stable ($\lambda < 0$). As the flow rate increases (the case $m = 5$), the cellular modes become also unstable within a certain interval of k. With a further increase in the flow rate, the growth rate of cellular instability increases while the oscillatory growth rate maxima decrease. For $m = 7$, for example, the growth rate of the cellular mode is approximately equal to the growth rate of the oscillatory mode. Finally, for $m = 9$, only the cellular modes remain unstable. One can see that with increasing values of m the growth rates for symmetric and nonsymmetric modes approach each other. Figure 14 shows also that for $Le < 1$ the highest growth rate for the oscillatory modes ($\lambda_I \neq 0$) always corresponds to a planar perturbation, $k = 0$.

Numerical modeling carried out in the framework of the two-dimensional model (all distributions are independent of z) showed that the flame dynamics for $Le = 0.9$ is similar to that for the case $Le = 1$ for moderately small values of m. Figure 15 shows the time histories for the flame position and the symmetry indicator calculated for the case $m = 4$. Two types of periodic dynamics were found. The first dynamics (a) is characterized by a weak amplitude for x_w and significant oscillations of S. It corresponds to a nonsymmetric mode. The second dynamics (b) corresponds to symmetric oscillations: S becomes equal to zero after a transient while the amplitude of x_w oscillates appreciably. It corresponds to a symmetric mode. The initial conditions for these numerical solutions were taken from the corresponding distributions obtained

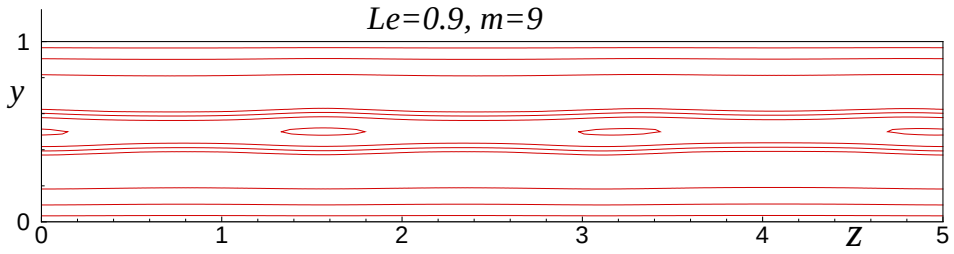

Figure 16. Temperature isolines in the slice $x = 5.825$; θ at intervals 0.25 calculated for $m = 9$, $Le = 0.9$ and $d = 15$.

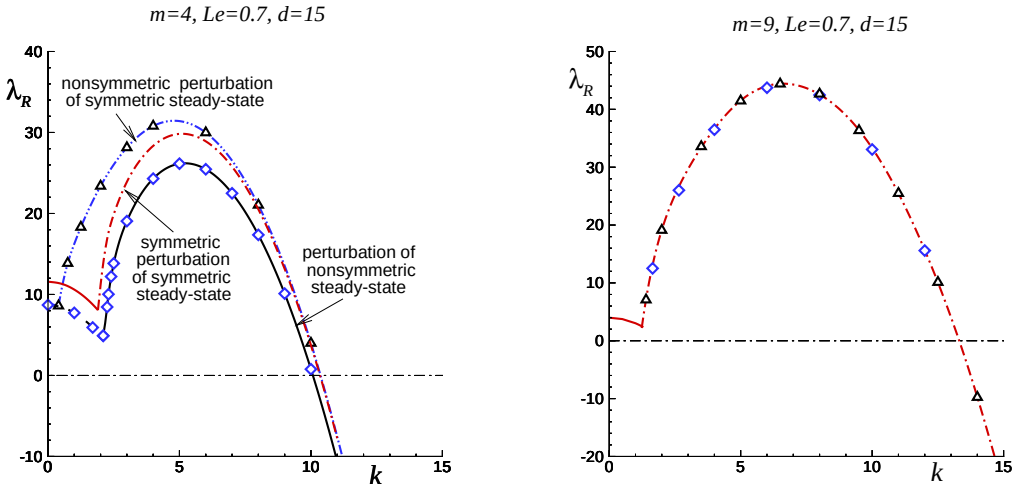

Figure 17. The growth rate of small perturbations, λ_R, as a function of the wave number k calculated for symmetric and nonsymmetric perturbations of symmetric steady-state solutions and for small perturbations of non-symmetric steady-state solutions; left plot - $m = 4$, right plot - $m = 9$, all the curves collapse into one; all curves calculated for $Le = 0.7$, $d = 15$ and $\theta_w = 0.6$.

for $Le = 1$. It can be seen that in both cases the periodic dynamics is sustained in time. It is assumed that these dynamics will be preserved in the framework of the three-dimensional model as for the case $Le = 1$, even if no calculations were performed. This can be concluded from Fig. 14 for $m = 4$ where possible cellular disturbances cannot arise because the corresponding (real) growth rate λ is less than zero.

With increasing intensity of the flow rate, m, the cellular structure of flames appears. Figure 16 shows the temperature isolines in a slice situated at $x = 5.825$ calculated for $m = 9$ and $Le = 0.9$ in three-dimensional simulations. The cells are clearly visible, but their intensity is quite small. The distance between cells is approximately $\ell \approx 1.65$, which corresponds to $k \approx 3.82$. This value is marked with an open circle in Fig. 14 for $m = 9$. It should be noted that the three-dimensional numerical simulation carried out for $m = 9$ shows, in addition to this cellular instability, weak oscillations with an amplitude x_w about 0.01. This can be attributed to nonlinear excitations of various unstable modes.

The stability analysis of steady-state solutions symmetrical with respect the channel midplane, $y = 1/2$, showed that these states are unstable in some cases. However, when

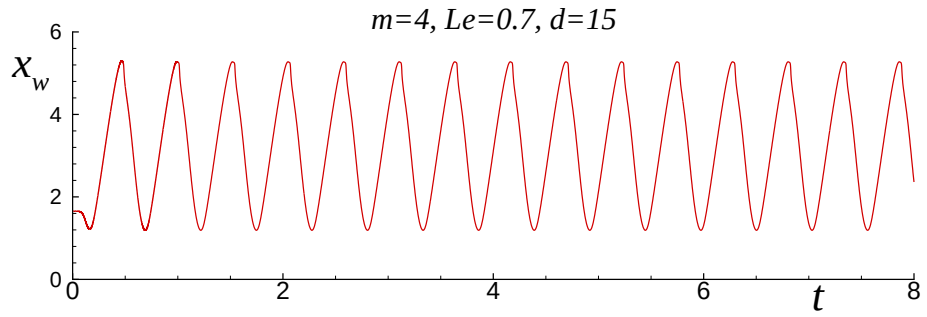

Figure 18. Time history of flame position x_w calculated for $m = 4$ and $Le = 0.7$ (obtained form 3D calculations).

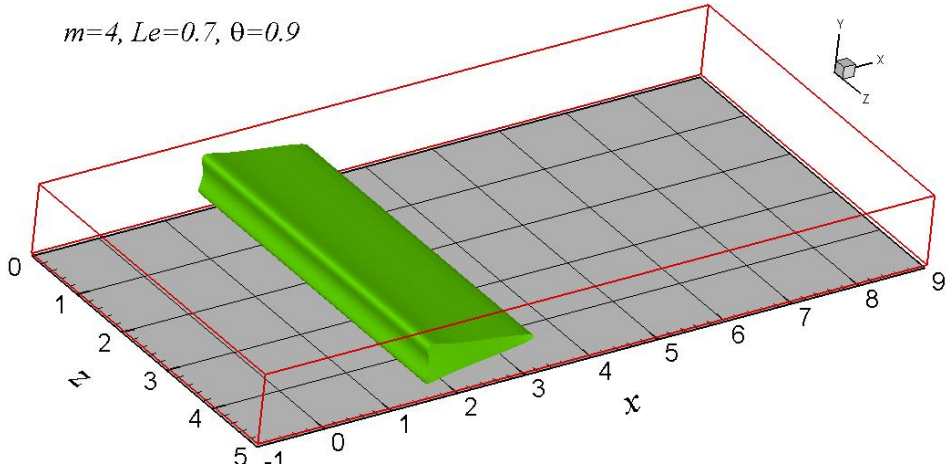

Figure 19. The instantaneous snapshot of the constant temperature surface, $\theta = 0.9$, calculated for $m = 4$ and $Le = 0.7$.

the Lewis number is sufficiently lower than unity, there exist also nonsymmetric steady-state solutions. The solutions of this type exist at least for $Le = 0.7$. An example is shown in Fig. 4. Stability of these solutions should also be considered.

In Fig. 17, we plot the growth rate λ_R for symmetric and nonsymmetric perturbations applied to the symmetric steady-state solutions as well as the growth rate of perturbations imposed to the nonsymmetric steady-state solutions. It can be seen that at moderately high flow rates ($m = 4$, the left plot), the curves differ from each other, although they have similar trends. However at higher flow rates the curves practically merge into one. For the case $m = 9$ in the right plot, the growth rate of nonsymmetric perturbations applied to the symmetric solution and the growth rate of perturbations applied to the nonsymmetric solution are shown by triangles and diamond symbols, respectively. It can be seen that despite some differences appearing at moderate m, the stability properties of the two steady-state solutions are very similar.

Because of the simultaneous existence of various unstable modes, it is almost impossible to be sure that in a specific implementation of a time-dependent calculation all possible non-steady solutions have been detected. There is always the possibility that, using different initial conditions, different time-dependent solutions can be found.

The following trend, observed in three-dimensional simulations, should be remarked.

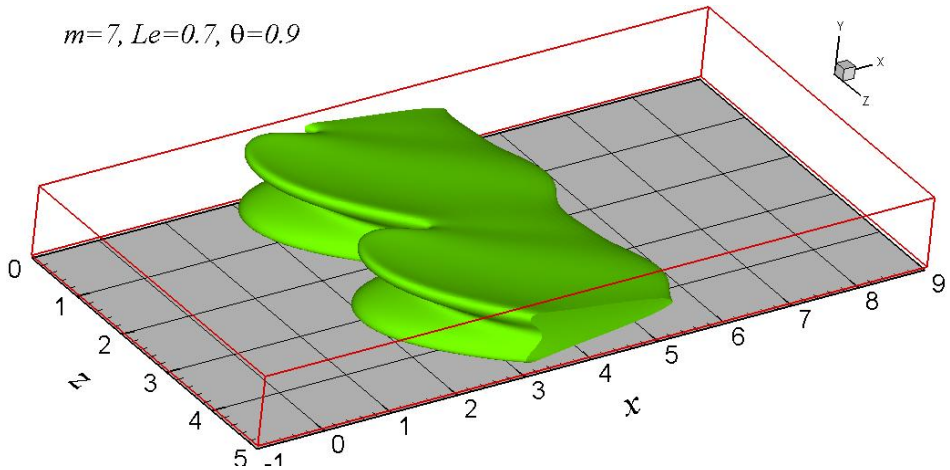

Figure 20. The instantaneous snapshots of the constant temperature surface, $\theta = 0.9$, calculated for $m = 7$ and $Le = 0.7$.

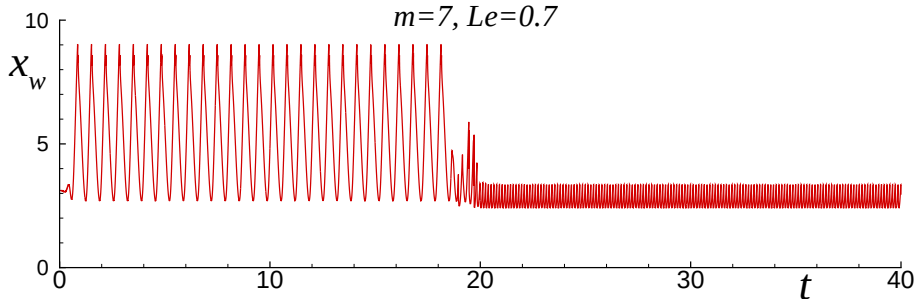

Figure 21. Time history of flame position, for $m = 7$ and $Le = 0.7$.

When large amplitude oscillations of x_w developed, the spatial distributions of variables became independent of the z-coordinate. This observation is supported by the stability analysis: the growth rate of the oscillatory instabilities has always a maximum at $k = 0$. In other words, during large amplitude oscillations of x_w, the cellular structure of the flame is suppressed.

Another unexpected observation can be made by comparing the results of stability analysis and the flame dynamics. It was detected that the magnitude of the growth rate of linear instabilities does not imperatively determine the flame dynamics observed in three-dimensional simulations. Figure 17 (left) shows that for $m = 4$ the growth rate of cellular instability exceeds the growth rate of oscillatory instability. Nevertheless, a numerical simulation of this case showed oscillations with a large amplitude in x_w and no cellular structure. The time history of x_w obtained in this simulation is shown in Figure 18. A snapshot of the flame shape is shown in Fig. 19 where a constant temperature surface is presented.

As the flow rate increases, an oscillating cellular flame structure appears. Figure 20 shows an instantaneous snapshot of the surface of constant temperature for the case $m = 7$ and $Le = 0.7$. Transition to this dynamics, occurred after an unexpectedly long time interval, as seen on Fig. 21. Up to $t \approx 18$, the flame presented large amplitude oscillations in x_w and a planar (independent of z) structure. After this time, the flame

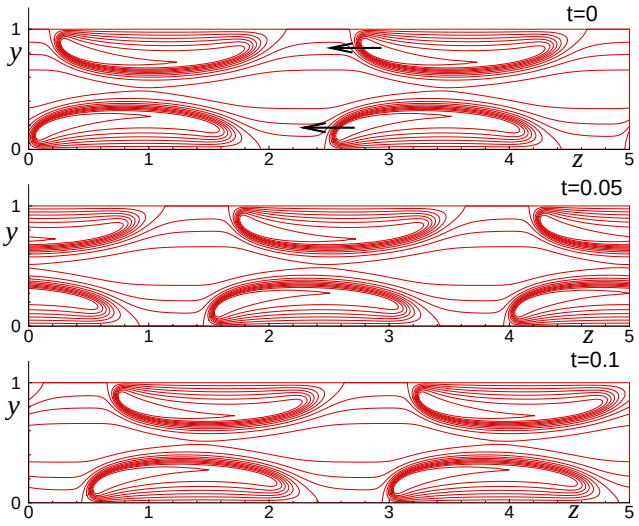

Figure 22. Snapshots of the temperature field for the first solution made at sequential times in the $x = 3.3$ plane for $m = 9$ and $Le = 0.7$. Both rows of cells move to the left.

dynamics was changed dramatically and a cell structure with significantly smaller amplitude oscillations in x_w appeared. The symmetry indicator S remains zero for the entire time shown in Fig. 21.

Interesting results were obtained in the three-dimensional simulations of the case with $m = 9$ and $Le = 0.7$. It was found that at least two different cellular flame dynamics can exist for the same set of parameters. Both solutions present two rows of cells. For the first solution, shown in Fig. 22, the upper and lower rows of cells move in the same transverse direction, say, synchronously. In the second solution, shown in Fig. 23, the upper and lower row of cells move in opposite directions. The direction of this motion is shown by arrows in the upper plots. It can also be seen that the hottest region in each cell points toward the direction of this movement. The three dimensional structure of the two solutions is shown by means of the $\theta = 0.9$ iso-surface in Figs. 24 and 25. Animations of these dynamics are included in supplementary material.

The differences in the dynamics of these two regimes can be seen in Fig. 26 where the flame position and the symmetry indicator are drawn as functions of time. The authors must admit that this result for $m = 9$ was obtained unintentionally by slight variations in the initial conditions. It remains completely unclear how the initial conditions, which are only slightly different from each other, result in so different periodic time-dependent solutions.

6. Discussions

Combustion in small-scale devices is a complex process that results from the combination of various physical phenomena and for which a small change in a single parameter may lead to a number of effects. One of the methods for understanding this process is the construction of simplified theoretical models. Often the simplifications adopted in these models look quite strong. However, these simplifications allow us to conduct analytical studies or to significantly accelerate the numerical simulations of the sys-

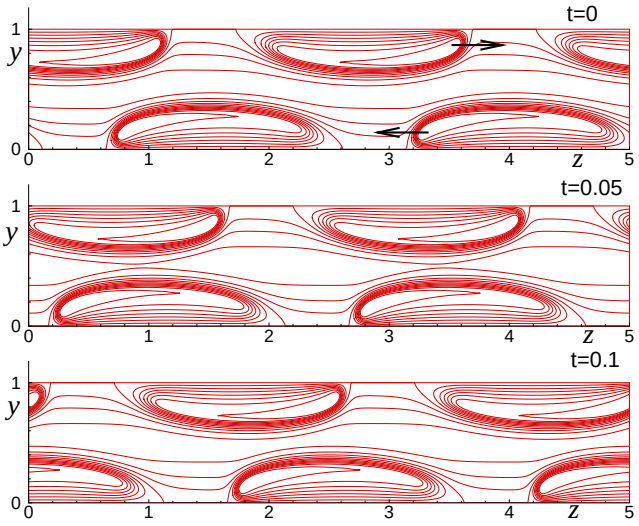

Figure 23. Snapshots of the temperature field for the second solution made at sequential times in the $x = 3.3$ plane for $m = 9$ and $Le = 0.7$. The upper row of cells moves to the right, the lower row to the left.

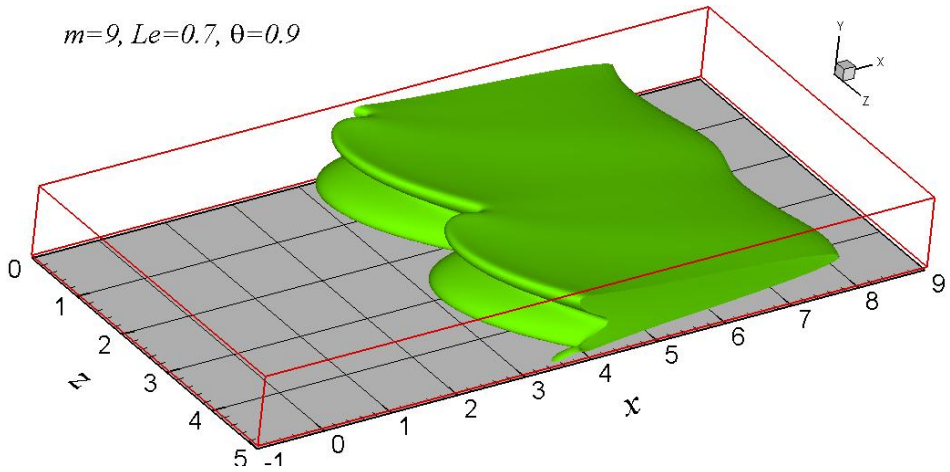

Figure 24. Snapshot of the temperature iso-surface, $\theta = 0.9$, for the first solution of the case $m = 9$ and $Le = 0.7$; the upper and lower row of cells move in the negative z-direction.

tem. We should be aware that the results obtained within these models indicate trends rather than predicting accurately quantitative measurements.

In the present work, premixed combustion in a narrow slot is studied in the framework of the constant-density model. The wall temperature is kept fixed and heated downstream. All these simplifications allowed not only to obtain steady and time-dependent solutions, but also to conduct the linear global stability analysis.

One of the unexpected results of this work is the multiplicity of time-periodic states. This effect was observed even for flames with a Lewis number equal to unity. It was shown that this is due to the simultaneous existence of two unstable modes of different types. One mode is symmetrical with respect to the channel midplane, while the other

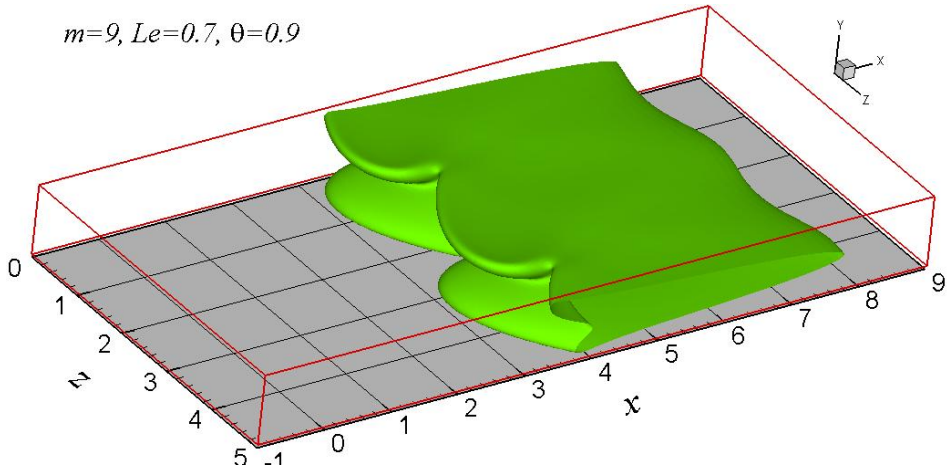

Figure 25. Snapshot of the temperature iso-surface, $\theta = 0.9$, for the second solution of the case $m = 9$ and $Le = 0.7$; the upper row of cells moves in the positive z-direction and the lower row moves in the negative z-direction.

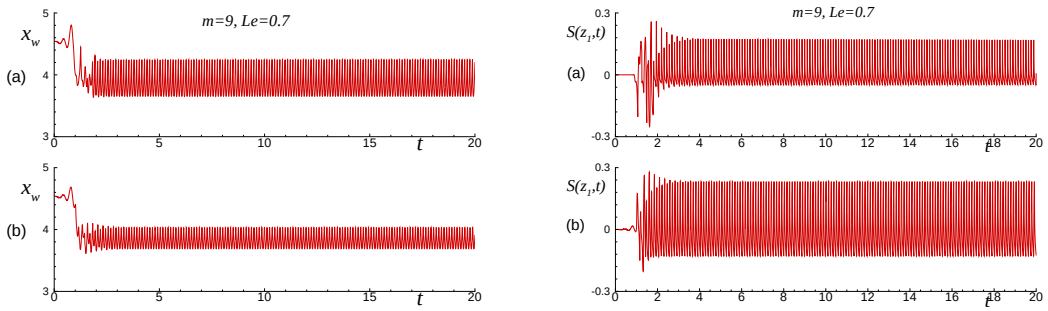

Figure 26. Time history of the flame position and the symmetry indicator for two regimes of cellular dynamics, calculated for $m = 9$ and $Le = 0.7$.

is nonsymmetric. The results showed that at certain values of the flow intensity, these modes do not interact with each other. However, at other values, mode mixing appears, leading to the emergence of complex oscillations.

These results can be of great importance in the analysis of experimental measurements and in their interpretation. It is obvious that the described phenomena can have a significant effect on the repeatability of experiments. Indeed, for the same values of the control parameters, different flame dynamics can be obtained in the same experiment.

Of course, important questions remain open. One of them is related to the experimental implementation of a particular regime of flame dynamics. As shown in this study, the emergence of a specific mode depends on the initial conditions. However, in a real experiment the initial conditions (usually an ignition event) are difficult to control. Another issue is the influence of effects not taken into account in the present model, such as, for example, the thermal expansion effect that would lead to variable density. One might expect that in rather narrow channels (the degree of narrowness

can be determined only by numerical experiments) the most important parameter will be the total mass flow rate, while density changes will not play a decisive role.

Finally, it should be added that even if the model adopted in this work introduces significant simplifications over more realistic models, it is hoped that at least some of the phenomena described here will be preserved under more general assumptions.

Acknowledgments

The authors acknowledge the support of Spanish MEC under Project #PID2019-108592RB-C42 / AEI / 10.13039/501100011033.

References

[1] A.C. Fernández-Pello, Micropower generation using combustion: issues and approaches, *Proc. Combust. Inst.* 29 (2002) 883-899 .

[2] D. Dunn-Rankin, E.M. Leal , D.C. Walther, Personal power systems, *Prog. Energy Combust. Sci.* 31 (2005) 422-465.

[3] K. Maruta, Micro and mesoscale combustion, *Proc. Combust. Inst.* 32 (2011) 125-150.

[4] Y. Ju, K. Maruta, Microscale combustion: technology development and fundamental research, *Prog. Energy Combust. Sci.* 37 (2011) 669-715 .

[5] D.C. Walther, J. Ahn, Advances and challenges in the development of power-generation systems at small scales, *Prog. Energy Combust. Sci.* 37 (2011) 583-610 .

[6] N.S. Kaisare, D.G. Vlachos, A review on microcombustion: fundamentals, devices and applications, *Prog. Energy Combust. Sci.* 38 (2012) 321-359 .

[7] S.A. Lloyd, F.J. Weinberg, A burner for mixtures of very low heat content, *Nature* 251 (1974) 47-49.

[8] S.A. Lloyd, F.J. Weinberg, Limits to energy release and utilisation from chemical fuels, *Nature* 257 (1975) 367-370.

[9] A.R. Jones, S.A. Lloyd, F.J. Weinberg, Combustion in heat exchangers, *Proc. R. Soc. Lond. A.* 360 (1978) 97-115.

[10] E.L. Belmont, S.M. Solomon, J.L. Ellzey, Syngas production from heptane in a non-catalytic counter-flow reactor, *Combust. Flame* 159 (2012) 3624-3631.

[11] D. Fernández-Galisteo, E. Fernández-Tarrazo, C. Jiménez, V.N. Kurdyumov, Analysis of an idealized counter-current microchannel-based reactor to produce hydrogen-rich syngas from methanol, *Int. J. Hydr. Eng.* 44 (2019) 23807-23820.

[12] V.N. Kurdyumov, Lewis number effect on the propagation of premixed flames in narrow adiabatic channels: Symmetric and non-symmetric flames and their linear stability analysis, *Combust. Flame* 158 (2011) 1307-1317.

[13] V.N. Kurdyumov, C. Jiménez, Propagation of symmetric and non-symmetric premixed flames in narrow channels: Influence of conductive heat-losses, *Combust. Flame* 161 (2014) 927-936.

[14] D. Fernández-Galisteo, C. Jiménez, M. Sánchez-Sanz, V.N. Kurdyumov, Effects of stoichiometry on premixed flames propagating in narrow channels: symmetry-breaking bifurcations, *Combust. Theory Modell.* 21 (2017) 1050-1065.

[15] A. Dejoan, C. Jimenez, V.N. Kurdyumov, Critical conditions for non-symmetric flame propagation in narrow channels: Influence of the flow rate, the thermal expansion, the Lewis number and heat-losses, *Combust. Flame* 209 (2019) 430-440.

[16] G. Pizza, C.E. Frouzakis, J. Mantzaras, A.G. Tomboulides, K. Boulouchos, Dynamics of premixed hydrogen/air flames in microchannels, *Combust. Flame* 152 (2008) 433-450.

[17] V.N. Kurdyumov, G. Pizza, C.E. Frouzakis, J. Mantzaras, Dynamics of premixed flames

in a narrow channel with a step-wise wall temperature, *Combust. Flame* 156 (2009) 2190-2200.

[18] G. Pizza, C.E. Frouzakis, J. Mantzaras, A.G. Tomboulides, K. Boulouchos, Three-dimensional simulations of premixed hydrogen/air flames in microtubes, *J. Fluid Mech.* 658 (2010) 463491.

[19] K. Maruta, T. Kataoka, N.I. Kim, S. Minaev, R. Fursenko, Characteristics of combustion in a narrow channel with a temperature gradient, *Proc. Combust. Int.* 30 (2005) 2429-2436.

[20] M. Hori, H. Nakamura, T. Tezuka, S. Hasegawa, K. Maruta, Characteristics of n-heptane and toluene weak flames in a micro flow reactor with a controlled temperature profile, *Proc. Combust. Int.* 34 (2013) 3419-3426.

[21] T. Kamada, H. Nakamura, T. Tezuka, S. Hasegawa, K. Maruta, Study on combustion and ignition characteristics of natural gas components in a micro flow reactor with a controlled temperature profile, *Combust. Flame* 161 (2014) 37-48.

[22] H. Nakamura, S. Suzuki, T. Tezuka, S. Hasegawa, K. Maruta, Sooting limits and PAH formation of n-hexadecane and 2,2,4,4,6,8,8-heptamethylnonane in a micro flow reactor with a controlled temperature profile *Proc. Combust. Int.* 35 (2015) 3397-3404.

[23] S. Takahashi, H. Nakamura, T. Tezuka, S. Hasegawaa, K. Maruta, Multi-stage oxidation of a CH2F2/air mixture examined by weak flames in a micro flow reactor with a controlled temperature profile, 201 (2019) 140-147.

[24] A.K. Dubeya, T. Tezukaa, S. Hasegawaa, H. Nakamuraa, K. Maruta, Analysis of kinetic models for rich to ultra-rich premixed CH4/air weak flames using a micro flow reactor with a controlled temperature profile, *Combust. Flame* 206 (2019) 68-82.

[25] V.N. Kurdyumov, C. Jimenez, Structure and stability of premixed flames propagating in narrow channels of circular cross-section: Non-axisymmetric, pulsating and rotating flames, *Combust. Flame* 167 (2016) 149-163.

[26] B. Denet , P. Haldenwang , A numerical study of premixed flames Darrieus-Landau instability, *Combust. Sci. Technol.* 104 (1995) 143-167 .